Atmospheric Environment 267 (2021) 118723

Contents lists available at ScienceDirect

Atmospheric Environment

journal homepage: www.elsevier.com/locate/atmosenv

# Contrasting aerosol growth potential in the northern and central-southern regions of the North China Plain: Implications for combating regional pollution

Yuying Wang [a,b,*], Jingling Wang [a], Zhanqing Li [c], Xiaoai Jin [b], Yele Sun [d], Maureen Cribb [c], Rongmin Ren [b], Min Lv [e], Qiuyan Wang [a], Ying Gao [a], Rong Hu [a], Yi Shang [a], Wanding Gong [a]

[a] Key Laboratory for Aerosol-Cloud-Precipitation of China Meteorological Administration, School of Atmospheric Physics, Nanjing University of Information Science & Technology, Nanjing, 210044, China
[b] State Key Laboratory of Remote Sensing Science, Beijing Normal University, Beijing, 100875, China
[c] ESSIC and the Department of Atmospheric and Oceanic Science, University of Maryland, College Park, MD, 20740, USA
[d] State Key Laboratory of Atmospheric Boundary Layer Physics and Atmospheric Chemistry, Institute of Atmospheric Physics, Chinese Academy of Sciences, Beijing, 100029, China
[e] School of Geographic Sciences, Nantong University, Nantong, 226000, China

## HIGHLIGHTS

- Diverse aerosol growth potentials were found in different regions of the North China Plain.
- Different particle growth mechanisms in winter and summer were reported.
- Distinct emission control measures are needed in different regions of the North China Plain to further improve air quality in the future.

## ARTICLE INFO

*Keywords:*
Aerosol
New particle formation
Particle growth
Haze formation
Emission control

## ABSTRACT

Aerosol growth potentials were investigated based on measurements of aerosol properties from three field campaigns carried out at sites in urban Beijing (BJ) and suburban Xingtai (XT) located in the North China Plain (NCP). BJ and XT were located in a northern megalopolis area and a central-southern industrial area, respectively, in the NCP. Results suggest new particle formation (NPF) events occurred more frequently, and the particle growth potential was greater in the central-southern NCP region than in the northern NCP region in summer. It is found that differences in primary emissions and meteorological conditions can cause regional and seasonal variations in aerosol growth potential in the NCP. Photochemical reactions were more important for particle growth in summer, while nocturnal aqueous chemical reactions were more important in winter. The large nocturnal particle growth rate (7.5 nm $h^{-1}$) was the reason inducing the severe aerosol pollution in winter BJ. Further analyses of submicron aerosol chemical species indicate more sulfate in submicron aerosols at XT, suggesting that the growth of new particles in the central-southern NCP in summer may be mainly dominated by the secondary formation of inorganics. Diurnal variations in aerosol chemical species during the three field campaigns suggest that the downward vertical mixing of nitrate over the nocturnal boundary layer played an important role in aerosol growth in the morning in summer. Moreover, the enhanced anthropogenic emissions during the late-day rush hours can cause clear increases in nitrate and organics. Our results highlight the distinct aerosol growth potentials in the northern and central-southern areas of NCP, implying that different emission control measures are needed in two regions to further improve air quality in the future.

* Corresponding author. Key Laboratory for Aerosol-Cloud-Precipitation of China Meteorological Administration, School of Atmospheric Physics, Nanjing University of Information Science & Technology, Nanjing, 210044, China.
*E-mail address:* yuyingwang@nuist.edu.cn (Y. Wang).

https://doi.org/10.1016/j.atmosenv.2021.118723
Received 20 May 2021; Received in revised form 7 September 2021; Accepted 11 September 2021
Available online 14 September 2021

## 1. Introduction

Aerosols, suspended matter in the atmosphere, have imperative impacts on human health, air quality, the ecosystem, and climate change (Fan et al., 2018; Z. Li et al., 2016, 2019; Rosenfeld et al., 2008; Shrivastava et al., 2017). Aerosol particles are either emitted by anthropogenic and natural sources or produced by gas-to-particle transformations. These primary and secondary particles can grow to large sizes through complex atmospheric physicochemical processes and are removed from the air through dry and wet deposition processes. A large number of gas precursors emitted by human activities (e.g., cooking, transportation, and industrial activities) can promote aerosol growth (Zhang et al., 2015; Guo et al., 2020). These growth processes can induce heavy haze events that are detrimental to human health and undermining socioeconomic development (Carmichael et al., 2009; Matus et al., 2012). Moreover, the growth of aerosols can change the particle size, a vital parameter dictating aerosol optical properties and activation of cloud condensation nuclei (CCN), which further changing local weather and even global climate (e.g., F. Zhang et al., 2017; Y. Wang et al., 2018; Li et al., 2019; Roldin et al., 2019; Williamson et al., 2019). Therefore, analyzing and comparing aerosol growth potential in different regions is important to gain an insight into the haze formation mechanism and aerosol-cloud interactions.

China, as the largest developing country, is facing tremendous challenges associated with air pollution and climate changes. The Chinese government, since 2013, has implemented a series of measures to hinder the formation of haze. These measures were effective in reducing primary pollutants in many areas of China (An et al., 2019; Q. Zhang et al., 2019). The concentrations of sulfur dioxide ($SO_2$), nitrous oxides ($NO_x$), and black carbon (BC) decreased by 59%, 21%, and 28%, respectively, from 2013 to 2017, but the concentrations of ammonium ($NH_3$) and non-methane volatile organic compounds exhibited a slight increase during these years (Zheng et al., 2018; Zhai et al., 2019). Meanwhile, the mass concentrations of particulate matter with an aerodynamic diameter of less than 2.5 μm ($PM_{2.5}$) decreased by 48%, 39%, and 32% in the three most economically developed regions, i.e., the Beijing-Tianjin-Hebei (BTH), Yangtze River Delta (YRD), and Pearl River Delta (PRD) regions, respectively, from 2013 to 2018 (J. Cheng et al., 2019; Vu et al., 2019; Wei et al., 2021). Nonetheless, the $PM_{2.5}$ reduction rate has slowed down in recent years due to the limiting of emission control measures and the enhancement of secondary processes (H. Li et al., 2019; Lei et al., 2020). It is thus necessary to take more stringent and scientific strategies to control secondary pollution in the future. More insights into the haze formation and particle growth mechanisms in China are thus warranted, which may also shed light to similar problems in other regions.

Numerous observational campaigns concerning aerosol properties have been conducted in China that are useful to study aerosol growth processes. Several new mechanisms were proposed based on those studies. For example, some studies found that high emissions and a strong atmospheric oxidation capacity can induce new particle formation (NPF) events and subsequent aerosol growth in many regions, important to haze formation (Guo et al., 2014; Huang et al., 2014; Z. Wang et al., 2017; Kulmala et al., 2021). Other studies have suggested that aqueous chemical reactions oxidized by nitrogen dioxide and nitrous acid are important to the formation of secondary aerosols (Cheng et al., 2016; G. Wang et al., 2016; Wang et al., 2020a). F. Zhang et al. (2020) have reported that BC catalytic chemistry dominates the formation and trend of regional haze, while Wu et al. (2020) proposed a new mechanism of new particle formation stressing the role of atmospheric turbulence. Peng et al. (2021) reviews recent advances in understanding secondary aerosol formation in the North China Plain (NCP), highlighting several critical chemical/physical processes, that is, new particle formation and aerosol growth driven by photochemistry and aqueous chemistry as well as the interaction between aerosols and atmospheric stability. Considering the diversity of emission sources and atmospheric conditions, these mechanisms have disparate impacts in different regions of China. The NCP is particularly susceptible to frequent occurrence of severe haze episodes. Aerosol growth potential in the NCP is complex due to the diverse anthropogenic emissions.

Particle number size distribution (PNSD) is a key quantity closely relating to aerosol growth processes, also echoing to some extent aerosol type, origin, and aging (Peng et al., 2014; Liang et al., 2020; Rivas et al., 2020). In recent years, many observational studies have been carried out in the NCP, investigating the PNSD (Du et al., 2017; Y. Zhang et al., 2018; Liang et al., 2020). However, most of these studies were based on measurements made at a single site in the northern megalopolis area of the NCP. Few studies have been conducted in the central-southern part of the NCP, which is one of the most intensive heavy industrial zones in China. To our knowledge, no study has compared the differences in PNSD patterns between the northern and central-southern NCP from which we may gain some unique understanding of aerosol growth processes. It is thus the focus of this study using the measurements of PNSD and aerosol chemical species from three field experiments at two representative sites in the northern and central-southern NCP. The PNSD patterns during the three campaigns and the factors contributing to the regional PNSD variations were investigated. Based on these analyses, we have gained a better knowledge of aerosol growth in the NCP which would help both understand and predict haze events.

This paper is organized as follows. Section 2 introduces sampling sites, field campaigns, instruments, and parameters of PNSD. Section 3 presents the results and discussion, including the comparison of PNSD patterns and parameters during the three field campaigns, as well as the impact of meteorological conditions and pollution emissions on aerosol growth processes in the NCP. Conclusions and summary are given in section 4.

## 2. Experiment and methodology

### 2.1. Observation sites and field campaigns

Beijing (BJ), the capital of China, is located in the northern part of the NCP, with a population of over 20 million. The terrain in BJ is elevated in the northwest and low in the southeast, surrounded by mountains to the west, north, and northeast. The BJ sampling site (Fig. 1) is located at the Institute of Atmospheric Physics, Chinese Academy of Sciences (39°97′ N , 116°37′ E , 49 m a.s.l.). The

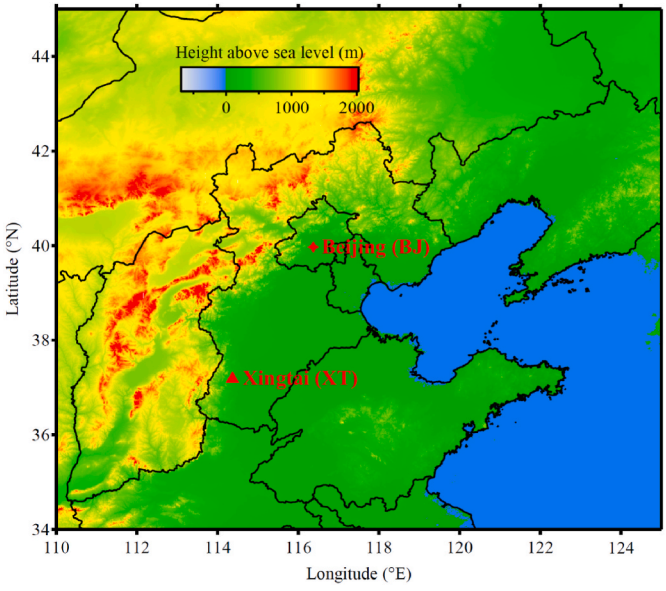


**Fig. 1.** Locations of the Beijing (BJ) and Xingtai (XT) sampling sites. The colored background shows the topographic heights.

surrounding area of this site is densely populated, with a large number of residential and recreational areas. Residential and surrounding road emissions are the main pollution sources here, representing the general emission situation in urban areas. As a highly urbanized mega-city, aerosol physical and chemical properties in Beijing have been studied extensively (e.g., Du et al., 2017; Shi et al., 2019; Wang et al., 2017, 2019). Under the auspices of the Atmospheric Pollution and Human Health in a Chinese Megacity (APHH-Beijing) program, two field campaigns measuring aerosol properties were carried out in BJ: in winter from 14 November to 22 December 2016 and in summer from 15 May to 30 June 2017 (Shi et al., 2019).

Another observation site is in the suburb of a small city named Xingtai (XT) in the central part of NCP and the southern part of Hebei province. Owing to the intense industrialization in this region with many manufactures, power plants, steal and grass etc., it is among the most polluted regions in China (Y. Wang et al., 2018; Y. Zhang et al., 2018). A field campaign called the Atmosphere–Aerosol–Boundary Layer–Cloud ($A^2BC$) Interaction Joint Experiment was carried out at XT in the summer from 30 April to 29 June 2016 (Li et al., 2019; Y. Wang et al., 2018) aimed at understanding: 1) physical, chemical, optical, hygroscopic and nucleation properties of anthropogenic aerosols; 2) aerosol and planetary-layer interaction; 3) aerosol-cloud interactions. The campaign site (Fig. 1) is a national weather station (37°11′ N, 114°22′ E, 180 m a.s.l.) located at the foothill of the Taihang Mt., about 17 km to the northwest of the XT urban area. Under weak atmospheric diffusion conditions, industrial pollutants are readily accumulated to cause severe air pollution (L. Wang et al., 2013). Aerosol and gas precursor concentrations in this region are generally high throughout the year. The XT site can thus be regarded as a typical industrial zone in the central-southern NCP.

### 2.2. Instrumentation

The scanning mobility particle sizers (SMPS) equipped with a long differential mobility analyzer (model 3081L, TSI Inc.) and two condensation particle counters (model 3772 in BJ and model 3776 in XT, TSI Inc.) were used to measure PNSD at the two sites, with the particle diameter ($D_p$) ranging from 13 to 552 nm in BJ and from 15 to 685 nm in XT. In this study, aerosol particles are divided into three modes, namely, the nucleation mode (15–40 nm), the Aitken mode (40–100 nm), and the accumulation mode (100–552 or 100–685 nm).

An Aerodyne aerosol mass spectrometer and an Aerodyne aerosol chemical speciation monitor were separately utilized at BJ and XT to measure the non-refractory submicron aerosol chemical species (sulfates, nitrates, chloride, ammonium, and organics). BC at both sites was measured by a seven-wavelength aethalometer (model AE-33, Magee Scientific Corp.). The mass concentration of BC was derived according to the absorption property of BC and attenuation degree of transmitted light. Y. Wang et al. (2018) and Shi et al. (2019) provide more information about the instruments deployed during the campaigns.

### 2.3. Parameterization

The PNSD is usually fitted with a multiple-mode log-normal function. Each mode is described by the following formula:

$$\frac{dN}{d\log D_p} = \frac{N_t}{\sqrt{2\pi}\log\sigma}\exp\left(-\frac{\left(\log D_p - \log\overline{D_p}\right)^2}{2(\log\sigma)^2}\right) \quad (1)$$

where $N_t$, $\overline{D_p}$, and $\sigma$ are the total particle number concentration, the median diameter, and the geometric mean standard deviation, respectively. The volume mean diameter ($D_v$) of the PNSD is calculated using the following equation:

$$D_v = \left(\frac{\int n(D_p) D_p^3 dD_p}{\int n(D_p) dD_p}\right)^{\frac{1}{3}} \quad (2)$$

The condensation sink ($CS$) is a parameter describing the condensation rate of vapor molecules on the surface of pre-existing aerosols. The magnitude of $CS$ is an important factor affecting the formation of new particles. In a high $CS$ environment, new particles are hard to form and grow (Kerminen et al., 2018). $CS$ is calculated by the following formula:

$$CS = 2\pi D \int_0^\infty D_p \beta_M(D_p) n(D_p) dD_p \quad (3)$$

$$= 2\pi D \sum_i \beta_M D_{p,i} N_i$$

$$\beta_M = \frac{K_n + 1}{0.377K_n + 1 + \frac{4}{3}\alpha^{-1}K_n^2 + \frac{4}{3}\alpha^{-1}K_n} \quad (4)$$

where $D$ is the diffusion coefficient of the condensing vapor, $\beta_M$ is the transitional correction factor, $D_{p,i}$ and $N_i$ are the particle diameter and the corresponding particle number concentration in the $i$th bin of the PNSD, respectively, $K_n$ is the Knudsen number, and $\alpha$ is the mass coefficient.

The growth rate ($GR$) of particles can be calculated using this formula:

$$GR = \frac{dD_p}{dt} = \frac{\Delta D_p}{\Delta t} = \frac{D_{p2} - D_{p1}}{t_2 - t_1} \quad (5)$$

where $D_{p2}$ and $D_{p1}$ are the representative particle diameters at times $t_1$ and $t_2$ respectively. In this study, we use the maximum-concentration method suggested by Kulmala et al. (2012) to calculate particle $GR$.

## 3. Results and discussion

### 3.1. Comparisons of PNSD from the three field campaigns

#### 3.1.1. Time series of PNSD

During the three field campaigns, variations in PNSD differed significantly (Fig. 2). During the winter observation period at BJ (Fig. 2a), seven haze events could be classified. The PNSD varied periodically, with PNCs gradually increasing then rapidly decreasing over a period of four to seven days (Guo et al., 2014). This was caused by cyclic changes in meteorological conditions and pollutant transportation (Y. Wang et al., 2017, 2019). During the two summer observation periods at BJ and XT (Fig. 2b and c), PNCs were much lower than that in winter at BJ, especially for accumulation-mode particles.

A typical NPF event involves an abrupt increase in nucleation-mode particles at its initial stage in the morning and subsequent growth of these new particles due to condensation and coagulation processes, showing a clear "banana" shape in the diurnal variation of the PNSD pattern (Lee et al., 2019; Kulmala et al., 2012). Fig. 2b and c suggest that NPF events occurred on some days in summer at BJ and XT. Particle sizes increased rapidly after the burst of nucleation-mode particles during those NPF events. The NPF events can be identified using the method provided by Dal Maso et al. (2005). Table S1 suggests that the NPF occurrence frequency (~48.08%) was higher (~48% in summer XT compared to ~46% and ~24% in winter and summer BJ, respectively), and the number of newly formed particles (particles with diameter less than 40 nm) was greater at XT than at BJ. This is possibly because XT is located in one of the industrial centers in the central-southern NCP, where there are more gas precursors [such as $SO_2$ and volatile organic compounds (VOCs)] and where the atmospheric oxidization capacity is stronger (Y. Wang et al., 2018; Y. Zhang et al., 2018). In addition, the

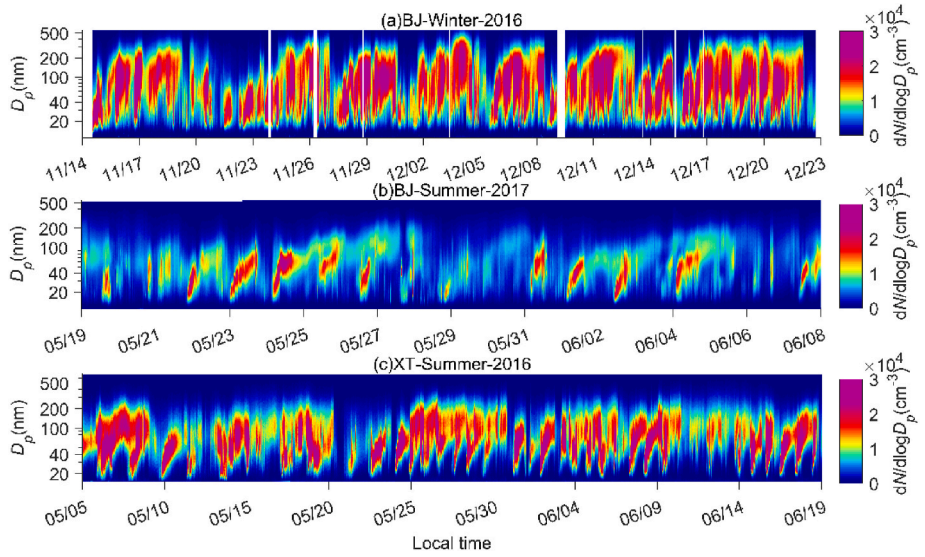


**Fig. 2.** Time series of aerosol particle number size distribution (PNSD) during the three field experiments at the BJ and XT sites: (**a**) 14 November to 22 December 2016 in BJ, (**b**) 19 May to 8 June 2017 in BJ, and (**c**) 5 May to 19 June 2016 in XT.

presence of amines and the high concentration of ammonia from agricultural emissions maybe the reason inducing the high frequency of NPF events (Zhang et al., 2010; Yao et al., 2018; Xiao et al., 2021).

### 3.1.2. *Diurnal variations in PNSD*

Fig. 3 compares the diurnal variations in PNSD, median particle diameter, *CS*, and *GR* during the three field campaigns. The PNC was lower, and the median particle diameter was smaller in summer than in winter at BJ. This is likely because the active planetary boundary layer (PBL) and good diffusion conditions in summer made the accumulation of particles difficult, especially those accumulation-mode particles. When the particles are small, they are easily coagulated by large particles. While, when these particles grow, they are less likely to be coagulated by large particles, thus keeping the PNC at a high level. Affected

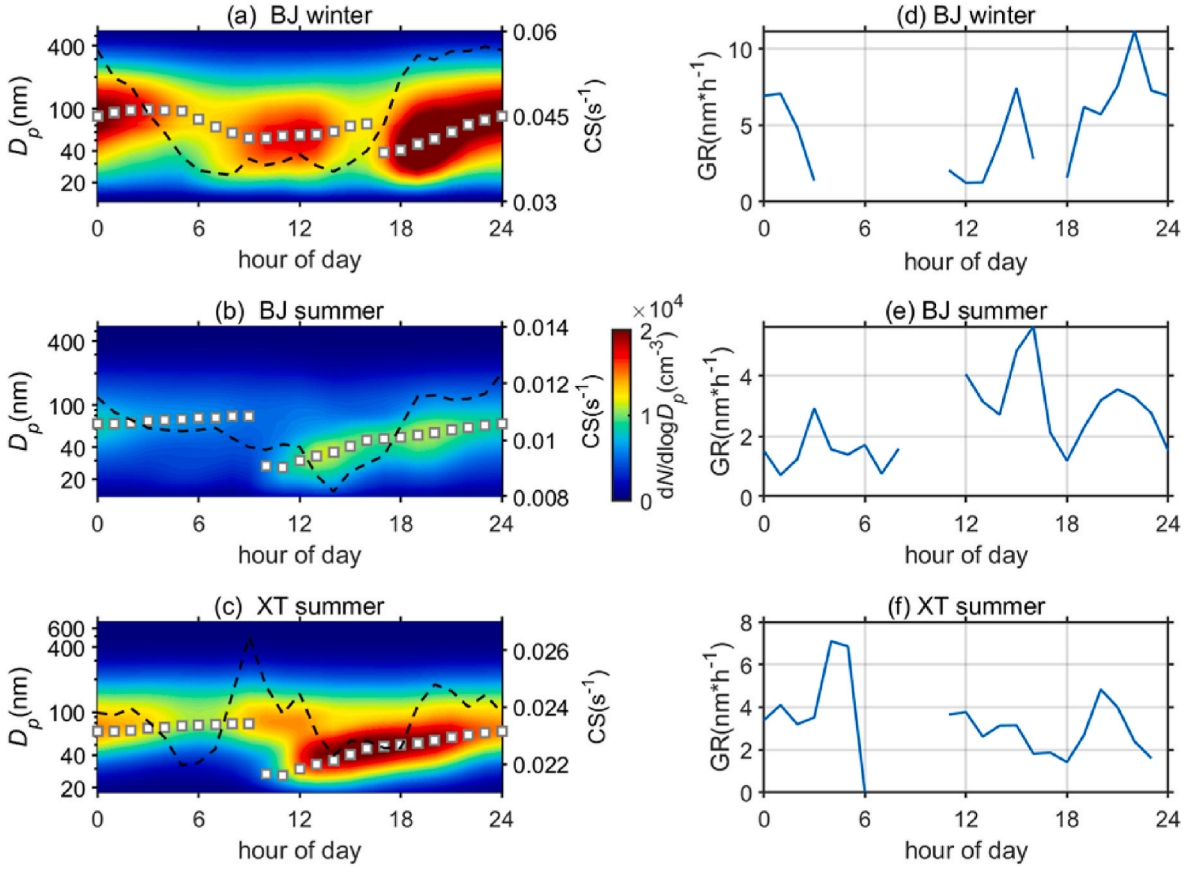


**Fig. 3.** Diurnal variations in PNSD (colored background), median particle diameter (white squares), condensation sink (*CS*, black dashed line), and growth rate (*GR*) during the three field campaigns.

by the massive emission of pollutants from traffic and cooking sources during the evening rush hour, PNCs increased significantly from 18:00 to 20:00 local time (LT) during the three field campaigns. Particles from primary emissions during these hours could be suspended in the air for a long time in winter, possibly due to the stable nocturnal PBL. Aqueous chemical reactions at night in winter both during NPF events and non-NPF events may have also promoted particle growth, maintaining high PNC levels all night long. For example, Wang et al. (2020a) found that the rapid oxidation of $SO_2$ by nitrogen dioxide ($NO_2$) and nitrous acid (HONO) takes place during a haze event from field observation, the formed sulfate shifts to larger particle sizes during the event, indicative of fog/cloud processing. Fig. S1 in the supplement suggests that the ambient RH could increase to a high level (>60%) at night during polluted periods in winter BJ. Previous studies (e.g., Jin et al., 2020) indicated that aerosol liquid water content (ALWC) could increase sharply when the RH was larger than 60% in winter BJ. The high content of ALWC would promote particle growth through aqueous chemical reactions. This further verify the important effect of aqueous chemical reactions on nocturnal particle growths.

The diurnal variations in *CS* during the three field campaigns also differed (Fig. 3). On the whole, affected by the differences in pollution levels and meteorological conditions, *CS* during the winter period was much higher than that during the summer period at BJ, and *CS* during the summer period at XT was in-between. Higher *CS* values usually corresponded to more accumulation-mode particles. The diurnal variation patterns of *CS* were similar during the winter and summer periods at BJ. In addition, Fig. S2 suggests that *CS* in the NPF days was always lower than that in the non-NPF days, especially in the morning. The lower *CS* in the morning was conducive to the occurrence of NPF events, particularly in summer, while the higher *CS* in the nighttime was conducive to aerosol condensational growth (Chu et al., 2019; Yao et al., 2018). The *CS* diurnal variation pattern at XT was different from that at BJ. *CS* fluctuated after sunrise in the morning, likely caused by the downward transportation of particles from the aerosol layer above the nocturnal PBL (Y. Wang et al., 2018). Many aged particles were gathered above the PBL in the nighttime at XT. After sunrise, upper particles were mixed into the boundary layer, increasing the PNCs of Aitken and accumulation modes in the short term (Fig. 3c) and leading to the rapid increase in *CS*. The vertical mixing effect of aged particles from the upper PBL and residual layer to near-surface in northern China has been verified by Huang et al. (2020) according to the observed and modeled results. With the further evolution of the PBL height in the morning, the PNC was diluted, and *CS* decreased significantly, which was beneficial to the occurrence of subsequent NPF events.

The diurnal variations in median particle size shown in Fig. 3 reveal that the growth time of particle differ in winter and summer. Fig. 3a shows that the median diameter grew quickly at night in winter BJ, implying that the nocturnal particle growth was obvious. In addition, this trend was synchronous with the rapid increase of RH (shown in Fig. S3), indicating the important role of aqueous chemical reactions on particle growth in the nighttime. The *GR* calculation result suggests that the max-concentration diameter increased from about 40 nm (18:00 LT) to 85 nm (24:00 LT) and the corresponding average *GR* was 7.5 nm $h^{-1}$ in winter BJ (Fig. 3d). During the same hours, the average *GR* in summer BJ and summer XT were 2.5 and 3.5 nm $h^{-1}$, respectively, suggesting the lower nocturnal particle growth in summer than in winter. This is because high ambient RH, a stable atmospheric environment (Zheng et al., 2015), and high concentrations of gas precursors (e.g., $NO_x$, $SO_2$, and VOCs) promoted strong aqueous chemical reactions, contributing to the fastest growth of particles from a few tens of nanometers to more than 100 nm at night in winter (G. Wang et al., 2016; Wu et al., 2018). In summer, the growth of particles occurred mainly in the daytime, which might be related with photochemical reactions. From 12:00 to 17:00 LT, the average *GR*s were 3.3, 3.7 and 3.0 nm $h^{-1}$ in winter BJ, summer BJ and summer XT, respectively.

### 3.1.3. Fitting curves and parameters of PNSDs

For further investigating the difference in aerosol pollution in different regions of the NCP, the mean PNSDs during the three field campaigns were fitted by three-mode log-normal distributions as described in Eq. 1. Fig. 4 shows the fitting curves and parameters in each mode, also listed in Table 1. Number concentrations of Aitken-mode and accumulation-mode particles were much higher than that of nucleation-mode particles during the winter observational period at BJ. As previously mentioned, this was caused by frequent haze events and the rapid growth of particle size due to nocturnal aqueous chemical reactions in winter. During the summer observational periods, the PNSD was dominated by Aitken-mode particles in BJ (Fig. S4), while it was dominated by accumulation-mode particles at XT, indicating different aerosol pollution levels between the northern and central-southern NCP regions in summer. Moreover, Fig. 4 and Table 1 also suggest that the number concentration of accumulation-mode particles at XT in summer was close to that at BJ in winter, although the diffusion conditions were better in summer than in winter. This indicates that the particle growth potential was greater in the central-southern NCP region although the average *GR* was lower. As described in section 2.1, the central-southern NCP region is highly industrialized and urbanized, so a large number of gas precursors from industrial sources were emitted into the air. The high concentration of accumulation-mode particles in this region was likely from the condensation and coagulation growth of ultrafine particles stemming from NPF events. By contrast, BJ is located in the northern NCP region with less industrial emissions, so particle growth in BJ in summer was weaker than that in XT.

### 3.1.4. vol mean diameters ($D_v$) of PNSDs

Fig. 5 shows the diurnal variations in the $D_v$s of PNSDs calculated by Eq. (2). The $D_v$s in summer at the two sites have unimodal diurnal variation patterns, with peak values of $D_v$ appearing between 06:00 to 10:00 LT after sunrise. This is probably due to the downward mixing effect of aged particles from the aerosol layer above the nocturnal PBL (Huang et al., 2020), which was discussed in section 3.1.2. With the high emission of traffic related-particles at rush hours and the outbreak of NPF events in the morning, the massive increase in ultrafine particles made $D_v$ decrease quickly, reaching a minimum value at ~1500 LT. Afterward, $D_v$ increased again with the aging of new particles.

By contrast, the $D_v$ in winter had a bimodal diurnal variation pattern, with two $D_v$ peaks appearing at about 04:00 and 17:00 LT. Strong aqueous chemical reactions at night in winter under high ambient RH and stable PBL conditions made particles grow rapidly, resulting in the appearance of the first $D_v$ peak in the early morning. Later, with the emission of primary aerosols during the morning rush hour, the increase in ultrafine particles made $D_v$ decrease significantly, and the first $D_v$ valley appeared from 10:00 to 14:00 LT. Afterward, with the enhancement of photochemical reactions in the afternoon, $D_v$ increased briefly and reached its second peak at about 16:00 LT. During the evening rush hour, $D_v$ decreased to its second valley value at about 20:00 LT due to the effect of primary emissions.

In summary, clear seasonal and regional variations in PNSD were seen in the NCP, likely caused by differences in pollutant sources and meteorological conditions. The different PNSD patterns led to the marked difference in *CS* values in summer and winter. Low *CS* values in summer were favorable to the occurrence of NPF events. NPF events were more frequent, and the particle growth potential was greater in the central-southern NCP region than in the northern NCP region. This was attributed to the high concentration of gas precursors emitted by industrial sources in the central-southern NCP region. Moreover, particle growth mechanisms were different in different seasons. Photochemical reactions dominated for particle growth in summer, while nocturnal aqueous chemical reactions dominated in winter. The influences of pollutant emissions and meteorological conditions on aerosol growth are discussed next.

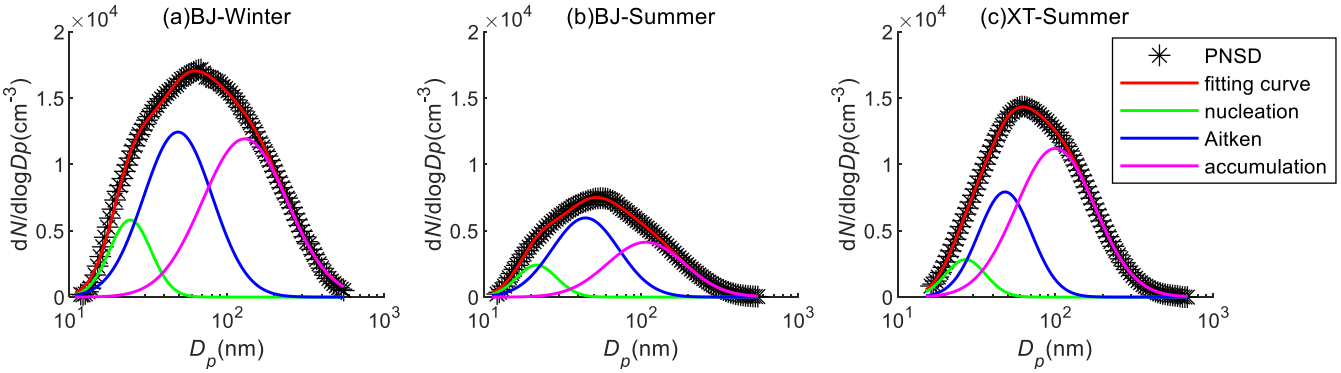


**Fig. 4.** Fitting curves of average PNSDs during the three field campaigns.

**Table 1**
Fitting parameters of average aerosol number size concentrations during the three field experiments.

| Mode | BJ-Winter-2016 | | | BJ-Summer-2017 | | | XT-Summer-2016 | | |
|---|---|---|---|---|---|---|---|---|---|
| | $N_t$ (cm$^{-3}$) | $\overline{D_p}$(nm) | $\sigma$ | $N_t$ (cm$^{-3}$) | $\overline{D_p}$(nm) | $\sigma$ | $N_t$ (cm$^{-3}$) | $\overline{D_p}$(nm) | $\sigma$ |
| Nucleation-mode | 1919 | 24.3 | 1.4 | 770.9 | 21.7 | 1.3 | 900 | 26.9 | 1.3 |
| Aitken-mode | 6824.8 | 49 | 1.7 | 3166.6 | 44.4 | 1.6 | 3338.7 | 47.9 | 1.5 |
| Accumulation-mode | 8045.1 | 130 | 1.9 | 2540.3 | 107.4 | 1.8 | 7019.5 | 100.1 | 1.8 |

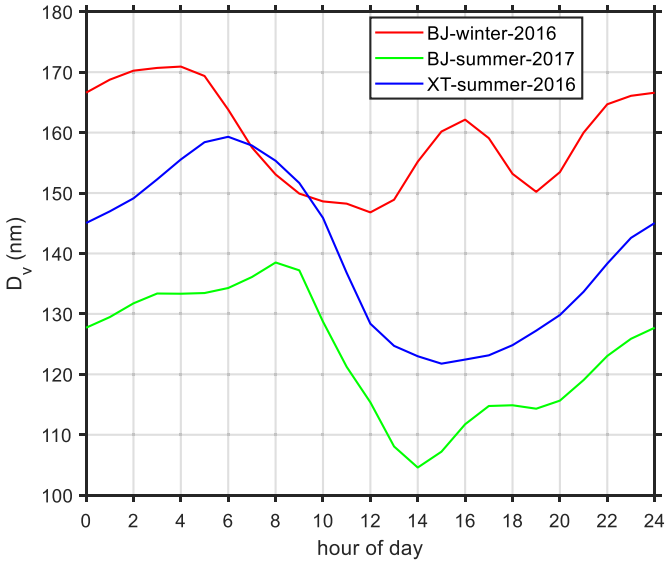


**Fig. 5.** Diurnal variations in volume mean diameters ($D_v$) of PNSDs during the three field campaigns.

### 3.2. Influence of meteorological conditions on aerosol growth

As reported in previous studies (Z. Wang et al., 2017; Chen et al., 2020), aerosol growth is greatly affected by meteorological conditions in the NCP. This section discusses the influences of ambient temperature, RH, and wind direction and speed on PNSD during the three field campaigns, indicating the possible impact of different meteorological variables on aerosol growth potential. Table 2 summarizes the average ambient temperature and RH during the three campaigns. The average temperature and RH were higher in summer than in winter at BJ. The higher RH in summer was conducive to aerosol hygroscopic growth, thus promoting the condensation and coagulation of particles. Compared with the summer observation period at BJ, the relatively lower temperature and higher RH in summer at XT were conducive to the occurrence of NPF events. This is because the molecular clusters formed by the condensation of gas precursors are hard decomposed and turn back into gases under lower ambient temperature and higher RH conditions, promoting the occurrence of NPF events (Chu et al., 2019; Lee et al., 2019). Therefore, meteorological conditions favorable to NPF events were one of the reasons for the high frequency of NPF events at XT, which has an important impact on aerosol growth potential.

**Table 2**
Mean temperature and relative humidity during the three observation periods.

| Site | Observation Time | Air Temperature (°C) | Relative Humidity (%) |
|---|---|---|---|
| BJ | 2016 Winter | 3.4 ( ±1.6 ) | 47.1 ( ±6.9 ) |
| BJ | 2017 Summer | 26.6 ( ±2.9 ) | 50.8 ( ±8.8 ) |
| XT | 2016 Summer | 23.2 ( ±2.9 ) | 53.0 ( ±9.4 ) |

Wind direction and speed determine the transportation of pollutants between different regions. As described in section 2.1, the northern and western parts of BJ are mountainous areas with a relatively sparse population and few pollution sources. Consequently, strong northwest winds can transport clean air from the northwest to the BJ urban area. However, the southern part of BJ (central and southern Hebei province) is a plain area with plentiful industrial sources. The transportation of industrial pollutants associated with southerly winds can increase the pollution level in the BJ urban area. The wind rose diagrams (Fig. 6a) depict the frequency distributions of winds during the three field campaigns. There were two prevailing winds at BJ in winter (Fig. 6a1), namely, winds from the south and from the northwest. The bivariate polar plot of submicron aerosols ($PM_1$) shown in Fig. 6b can be used to detect potential emission sources (Carslaw and Beevers, 2013). It shows two sources contributed considerably to the $PM_1$ accumulation at BJ in winter (Fig. 6b1): one source being the local emission sources, like traffic and cooking emissions; another source being the remote transportation of pollutants from the south. When the wind is from the south and light, the PBL is stable over BJ in winter, and air pollutants tend to accumulate, easily causing heavy haze events (Z. Li et al., 2017; Su et al., 2020). However, strong northwestern winds can bring in clean air, easily dispersing accumulated pollutants. The transition between the two prevailing winds in winter would sharply change the pollution situation at BJ, resulting in dramatic variations in PNSD patterns between clean and polluted periods (Fig. 2a), a leading cause for the sawtooth-like variations in aerosol optical depth observed in the region

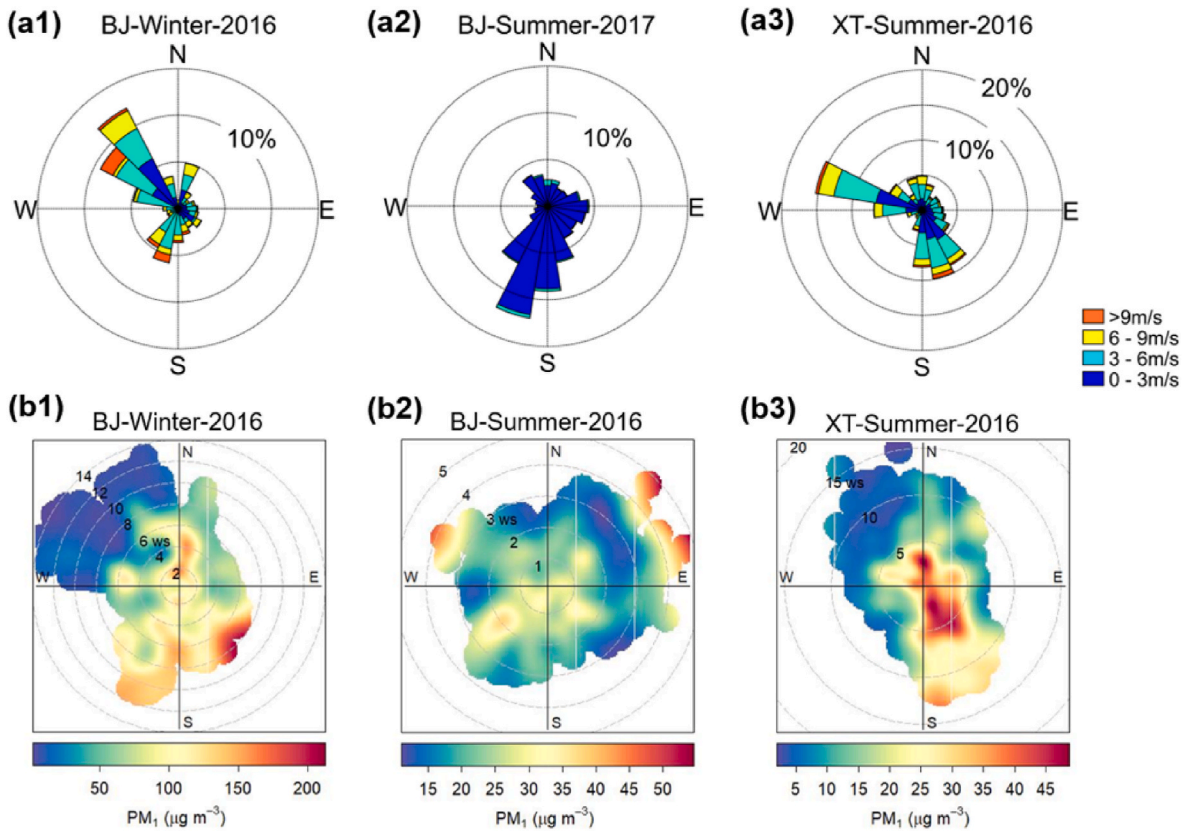


**Fig. 6.** (**a1-a3**) Wind rose diagrams and (**b1-b3**) bivariate polar plot of submicron aerosols ($PM_1$) for the three field experiments. The color scale in (**b1-b3**) shows the mass concentration of $PM_1$ in μg $m^{-3}$ and the radial scale shows wind speed, which increases from the center of the plot radially out-wards. (For interpretation of the references to color in this figure legend, the reader is referred to the Web version of this article.)

(Li et al., 2007). By contrast, the prevailing winds in summer at BJ were light easterly and southerly winds (Fig. 6a2). These winds could carry a large number of gas precursors to the observation site, favoring NPF events. However, the PBL in summer was active, so particles could not accumulate for long periods. The air was thus clear most of the time during the summer observation period at BJ, and the PNC was much lower than that in winter. Fig. 6b2 suggests the sources of $PM_1$ were diverse at BJ in Summer.

Compared with BJ, the special geographical location of XT at the foot of the Taihang Mt. with an altitude much lower than those of surrounding cities (Y. Zhang et al., 2018), the dispersion conditions of pollutants at XT were poor, and pollutants easily accumulated. Fig. 6a3 shows that the wind was mostly from the west and southeast in summer at XT, with wind speeds generally less than 6 m/s. Although there was a strong northwesterly airflow, this did not change the state of the pollution situation at this site. This is because XT is located in one of the centers of industrial pollution, with a large number of pollutants transported to this site no matter the wind direction. Therefore, XT remained highly polluted for a long time, even in summer. The high concentration of gas precursors and strong atmospheric oxidation capacity promoted the frequent occurrence of NPF events at XT, although the *CS* was higher at this site than at BJ. Kulmala et al. (2017) suggests that the NPF occurrence is affect by both *CS* and cluster growth rate, and the cluster growth rate is closely related to the gas precursors. Fig. 6b3 depicts that local sources contributed most to $PM_1$ at XT in summer. This implies that NPF events play an important role in the haze formation in the industrial regions of central-southern NCP.

In short, haze formation and dispersal were closely related to the change in winds in the northern NCP region (represented by the BJ site) in winter, while good atmospheric diffusion conditions were not conducive to the formation of heavy pollution events in summer. The meteorological conditions in the central-southern NCP region (represented by the XT site) in summer were favorable for the occurrence of NPF events, and the resulting large number of new particles and their aging growth made air pollution in this region more serious than that in the northern NCP region. All this indicates the different impacts of meteorological conditions on aerosol growth processes in the northern and central-southern NCP.

### 3.3. *Influence of primary emissions on aerosol growth*

Primary emissions are one of the important factors determining aerosol chemical composition. Simultaneous measurements of aerosol chemical composition and the PNSD can be used to study the characteristics of primary emissions and their effect on growth processes. The pie charts in Fig. 7 suggest that the mass fraction of organics (Org) was the largest in $PM_1$ during the three field campaigns, followed by sulfate ($SO_4^{2-}$) or nitrate ($NO_3^-$), and then ammonium ($NH_4^+$), BC, and chloride ($Cl^-$). The mass fraction of sulfate at BJ in summer (~21%) was higher than that in winter (~13%). This is likely because the strong photochemical reactions in summer were favorable to the formation of sulfate. However, the mass fraction of sulfate at XT in summer was higher than that at BJ, which was related to more $SO_2$ emissions from industrial coal combustion in the central-southern NCP region. Previous studies suggest that the conversion of $SO_2$ to $H_2SO_4$ and then be neutralized by $NH_3$ due to photochemical reactions plays a major role in aerosol nucleation and growth (e.g., Peng et al., 2014; Lee et al., 2019; Stolzenburg et al., 2020), so more industrial emissions of $SO_2$ may be one of the causes for more NPF events and more accumulation-mode particles at XT in summer. By contrast, the mass fraction of nitrate in summer was lower than that in winter, possibly because nitrate was easy to volatilize under high ambient temperature conditions in summer (Y. Li et al., 2017; Wang

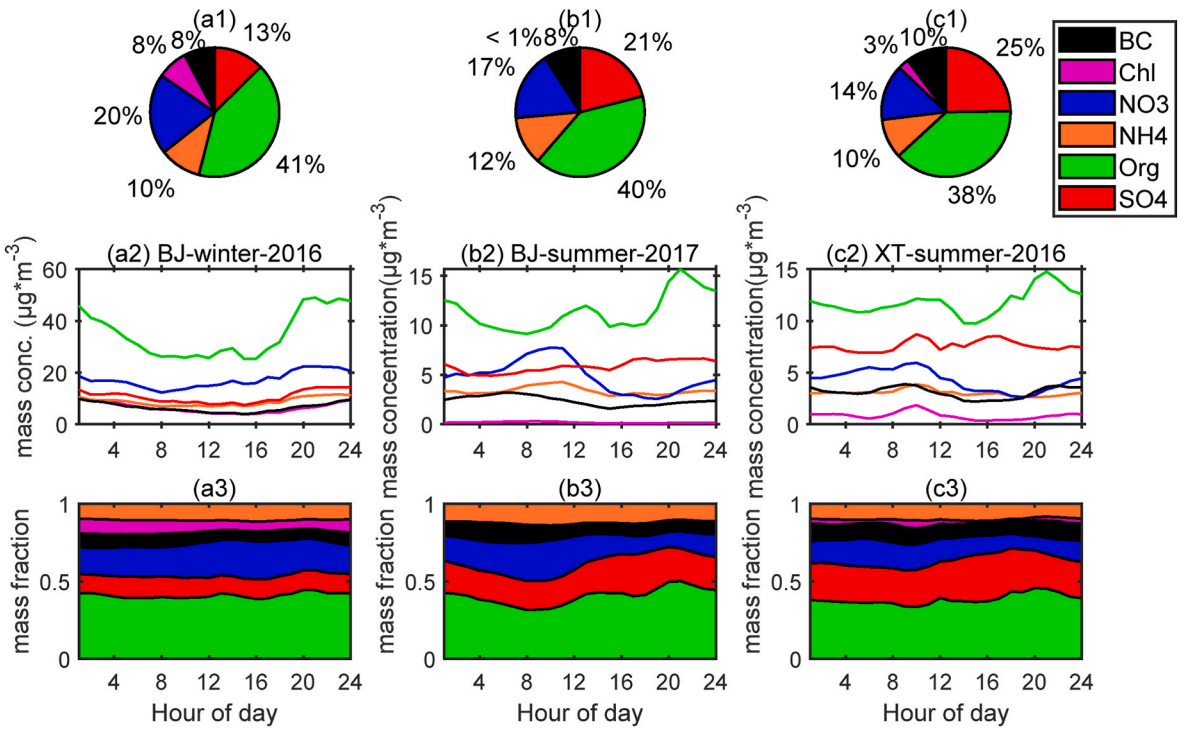


**Fig. 7.** Average mass percentages (a1-c1), diurnal variations in mass concentrations (a2-c2) and mass fractions (a3-c3) of aerosol chemical species during the three field campaigns.

et al., 2020b).

Fig. 7 also depicts the diurnal variations in mass concentrations ($m$) of different aerosol chemical species in $PM_1$ during the three field campaigns. The $m$ of every aerosol chemical species clearly increased in the evening (especially the $m$ of organics and nitrate), caused by massive emissions of primary pollutants during the late-day rush hours and the enhancement of aqueous chemical reactions as the PBL height decreased. However, the increased ambient RH at night could also strengthen the coagulation scavenging of particles, so the $m$ of most aerosol chemical species decreased gradually in the early morning until around sunrise the next day. All these phenomena could cause the PNSD variations shown in Fig. 3. Fig. 7 also shows that the diurnal variation in nitrate mass concentration ($m_{NO_3}$) in different seasons was different. Affected by the diurnal variation in ambient temperature, $m_{NO_3}$ reached its peak in the morning in summer. Fig. 5 shows that the $D_v$ also reached its peak in the morning in summer, and its diurnal variation pattern was similar to that of $m_{NO_3}$. This indicates that residual aerosols over the nocturnal boundary layer in summer likely contained many nitrates, making particle sizes increase remarkably in the short term with the lifting of the PBL height in the morning. This is consistent with the modeled and observed results in northern China by Huang et al. (2020). After sunrise, the volatilization of nitrate was enhanced as the ambient temperature increased. The common influences of nitrate volatilization and NPF outbreak made particle sizes decrease quickly in the morning in summer (Fig. 5). However, the peak of $m_{NO_3}$ in winter occurred in the evening, and its diurnal variation was weaker than that in summer. The $m$s of other aerosol chemical species (sulfate, ammonium, and chlorine) show relatively weak diurnal variations, with small increases during rush hour. Particularly, the mass fraction of sulfate increased significantly in the daytime at XT. This further verifies that frequent NPF events and subsequent particle growth were closely related to massive emissions of $SO_2$ in the central-south region of the NCP.

In conclusion, the main aerosol chemical species in the northern and central-southern NCP were consistent, mainly comprised of organics and secondary inorganics. However, the mass concentrations and fractions of aerosol chemical species in different regions and seasons were different, implying different aerosol sources and ageing processes. The stable atmospheric environment and low ambient temperature in winter promoted the growth of primary and secondary aerosols, which can increase the number concentration of accumulation-mode particles during haze events. Favorable atmospheric diffusion conditions were not conducive to the occurrence of heavy haze events in summer but were conducive to the occurrence of NPF events due to strong photochemical reactions. The metropolitan area in the northern NCP was greatly affected by anthropogenic emissions, and the mass of nitrate accounted for a larger proportion of inorganic salts. Nitrate and organic matter were the main chemical species for particle growth. By contrast, the central-southern region of NCP was greatly affected by industrial emissions. More $SO_2$ in this region was beneficial to the occurrence of NPF events, leading to more sulfate formation in $PM_1$ in this region.

## 4. Summary and conclusions

The North China Plain (NCP) is one of the areas of the world with a dense population and heavy industrial activities, where aerosol pollution is complex and diverse. In this study, aerosol growth potential in the north and central-south regions of the NCP were compared based on measurements of aerosol properties from three field campaigns carried out at the urban Beijing (BJ) and suburban Xingtai (XT) sites. BJ is located in the northern megalopolis area of the NCP, while XT is located in the central-southern industrial area of the NCP.

It is found that differences in primary emissions and meteorological conditions can cause regional and seasonal variations in aerosol growth potential in the NCP. First, aerosol growth mechanisms were different in different seasons. Photochemical reactions were more important for particle growth in summer, while nocturnal aqueous chemical reactions were more important in winter. Second, NPF events were more frequent, and the particle growth potential was greater in the central-southern NCP region than in the northern NCP region, resulting in more severe aerosol pollution in the central-southern NCP in summer. This was attributed to meteorological conditions favorable to aerosol growth processes and the high concentration of gas precursors from industrial

emissions in the central-southern NCP. In winter, the formation and dispersal of haze events were inextricably linked to the change in wind direction contributed by local and remote sources in the northern NCP region, showing that weak southern winds transporting air masses with high ambient RH were conducive to aerosol growth, while strong northern winds transporting clean air masses could promote the diffusion of aerosol pollutants.

Aerosol chemical compositions in $PM_1$ during the three field campaigns were further investigated. Nitrate and organic matter were the main chemical species for particle growth, especially in winter in the northern NCP. Residual aerosols over the nocturnal boundary layer in summer likely contained many nitrates in summer in the NCP. The vertical mixing of nitrate with the elevation of the PBL height in the morning played an important role on the aerosol growth in the morning. Photochemical reactions in summer were favorable to the formation of sulfate, leading to the large mass fraction of sulfate in $PM_1$ in summer. The high concentration of $SO_2$ from coal combustion may be the reason causing the frequent NPF events and subsequent particle growth in the central-southern NCP, leading to the increase in sulfate mass concentration in the daytime in summer. By contrast, the metropolitan area in the northern NCP was greatly affected by anthropogenic emissions, and the mass of nitrate accounted for a large proportion of inorganic salts.

All these results reveal the distinct aerosol growth potential in the northern and central-southern regions of NCP, which can cause variations in the PNSD. This implies that different emission controls are needed to hinder regional hazes in different regions of NCP. A further reduction in coal emission is still necessary in the central-southern industrial region, which will be beneficial to improve air quality in the north due to the decrease in the cross-region transport of pollutants. The control of anthropogenic primary emissions (such as vehicle and cooking emissions) is also needed in the northern megalopolitan region, especially during the periods with weak diffusion conditions.

## Credit author statement

YW and JW led this work and prepare this paper; ZL designed the experiment and helped improving the quality of this paper; YW, XJ and YS participated in the taken of three field campaigns and processed the measurement data; MC copyedited the article. RR, ML, QW, YG, RH, and WG participated the discussion and figure processing in this paper.

## Declaration of competing interest

The authors declare that they have no known competing financial interests or personal relationships that could have appeared to influence the work reported in this paper.

## Acknowledgements

This work was funded by the National Natural Science Foundation of China (NSFC) research projects (grant no. 42030606, 42005067, 41705125), the National Key R&D Program of the Ministry of Science and Technology, China (grant no. 2017YFC1501702), and the Open Fund of State Key Laboratory of Remote Sensing Science (grant no. 202015). We also thank all participants in the three field campaigns for their tireless work and cooperation. The associated data can be downloaded online (https://drive.google.com/file/d/1Maqh8J3uSiwsQEicqkLf6BO_iHpLoLVc/view?usp=sharing).

## Appendix A. Supplementary data

Supplementary data to this article can be found online at https://doi.org/10.1016/j.atmosenv.2021.118723.

## References

An, Z., Huang, R., Zhang, R., Tie, X., Li, G., Cao, J., Zhou, W., Shi, Z., Han, Y., Gu, Z., Ji, Y., 2019. Severe haze in northern China: a synergy of anthropogenic emissions and atmospheric processes. Proc. Natl. Acad. Sci. U. S. A 116, 8657. https://doi.org/10.1073/pnas.1900125116.

Carmichael, G.R., Adhikary, B., Kulkarni, S., D Allura, A., Tang, Y., Streets, D., Zhang, Q., Bond, T.C., Ramanathan, V., Jamroensan, A., Marrapu, P., 2009. Asian aerosols: current and year 2030 distributions and implications to human health and regional climate change. Environ. Sci. Technol. 43, 5811–5817. https://doi.org/10.1021/es8036803.

Carslaw, D.C., Beevers, S.D.(, 2013. Characterising and understanding emission sources using bivariate polar plots and k-means clustering. Environ. Model. Software 40, 325–329. https://doi.org/10.1016/j.envsoft.2012.09.005.

Chen, Z., Chen, D., Zhao, C., Kwan, M., Cai, J., Zhuang, Y., Zhao, B., Wang, X., Chen, B., Yang, J., Li, R., He, B., Gao, B., Wang, K., Xu, B.(, 2020. Influence of meteorological conditions on $PM_{2.5}$ concentrations across China: a review of methodology and mechanism. Environ. Int. 139 https://doi.org/10.1016/j.envint.2020.105558.

Cheng, Y., Zheng, G., Wei, C., Mu, Q., Zheng, B., Wang, Z., Gao, M., Zhang, Q., He, K., Carmichael, G., 2016. Reactive nitrogen chemistry in aerosol water as a source of sulfate during haze events in China. Sci. Adv. 2, e1601530.

Cheng, J., Su, J., Cui, T., Li, X., Dong, X., Sun, F., Yang, Y., Tong, D., Zheng, Y., Li, Y., Li, J., Zhang, Q., He, K., 2019. Dominant role of emission reduction in $PM_{2.5}$ air quality improvement in Beijing during 2013–2017: a model-based decomposition analysis. Atmos. Chem. Phys. 19, 6125–6146. https://doi.org/10.5194/acp-19-6125-2019.

Chu, B., Kerminen, V.M., Bianchi, F., Yan, C., Petäjä, T., Kulmala, M., 2019. Atmospheric new particle formation in China. Atmos. Chem. Phys. 19, 115–138. https://doi.org/10.5194/acp-19-115-2019.

Dal Maso, M., Kulmala, M., Riipinen, I., Wagner, R., 2005. Formation and growth of fresh atmospheric aerosols: eight years of aerosol size distribution data from SMEAR II, Hyytiälä, Finland. Boreal Environ. Res. 10, 323–336.

Du, W., Zhao, J., Wang, Y., Zhang, Y., Wang, Q., Xu, W., Chen, C., Han, T., Zhang, F., Li, Z., Fu, P., Li, J., Wang, Z., Sun, Y., 2017. Simultaneous measurements of particle number size distributions at ground level and 260 m on a meteorological tower in urban Beijing, China. Atmos. Chem. Phys. 17, 6797–6811. https://doi.org/10.5194/acp-17-6797-2017.

Fan, J., Rosenfeld, D., Zhang, Y., Giangrande, S.E., Li, Z., Machado, L.A.T., Martin, S.T., Yang, Y., Wang, J., Artaxo, P., Barbosa, H.M.J., Braga, R.C., Comstock, J.M., Feng, Z., Gao, W., Gomes, H.B., Mei, F., Pöhlker, C., Pöhlker, M.L., Pöschl, U., de Souza, R.A.F.(, 2018. Substantial convection and precipitation enhancements by ultrafine aerosol particles. Science 359, 411. https://doi.org/10.1126/science.aan8461.

Guo, S., Hu, M., Zamora, M.L., Peng, J., Shang, D., Zheng, J., Du, Z., Wu, Z., Shao, M., Zeng, L., Molina, M.J., Zhang, R.(, 2014. Elucidating severe urban haze formation in China. Proc. Natl. Acad. Sci. U. S. A 111 (17). https://doi.org/10.1073/pnas.1419604111, 373–17,378.

Guo, S., Hu, M., Peng, J., Wu, Z., Zamora, M.L., Shang, D., Du, Z., Zheng, J., Fang, X., Tang, R., Wu, Y., Zeng, L., Shuai, S., Zhang, W., Wang, Y., Ji, Y., Li, Y., Zhang, A.L., Wang, W., Zhang, F., Zhao, J., Gong, X., Wang, C., Molina, M.J., Zhang, R.(, 2020. Remarkable nucleation and growth of ultrafine particles from vehicular exhaust. Proc. Natl. Acad. Sci. U. S. A 117, 3427. https://doi.org/10.1073/pnas.1916366117.

Huang, R., Zhang, Y., Bozzetti, C., Ho, K., Cao, J., Han, Y., Daellenbach, K.R., Slowik, J. G., Platt, S.M., Canonaco, F., Zotter, P., Wolf, R., Pieber, S.M., Bruns, E.A., Crippa, M., Ciarelli, G., Piazzalunga, A., Schwikowski, M., Abbaszade, G., Schnelle-Kreis, J., Zimmermann, R., An, Z., Szidat, S., Baltensperger, U., Haddad, I.E., Prévôt, A.S.H., 2014. High secondary aerosol contribution to particulate pollution during haze events in China. Nature 514, 218–222. https://doi.org/10.1038/nature13774.

Jin, X., Wang, Y., Li, Z., Zhang, F., Xu, W., Sun, Y., Fan, X., Chen, G., Wu, H., Ren, J., Wang, Q., Cribb, M., 2020. Significant contribution of organics to aerosol liquid water content in winter in Beijing, China. Atmos. Chem. Phys. 20, 901–914. https://doi.org/10.5194/acp-20-901-2020.

Kulmala, M., Petäjä, T., Nieminen, T., Sipilä, M., Manninen, H.E., Lehtipalo, K., Dal Maso, M., Aalto, P.P., Junninen, H., Paasonen, P., Riipinen, I., Lehtinen, K.E.J., Laaksonen, A., Kerminen, V.-M., 2012. Measurement of the nucleation of atmospheric aerosol particles. Nat. Protoc. 7 (9), 1651–1667. https://doi.org/10.1038/nprot.2012.091.

Kulmala, M., Kerminen, V.M., Petj, T., Ding, A., Lin, W., 2017. Atmospheric Gas-to-Particle Conversion: why NPF events are observed in megacities? Faraday Discuss 200.

Kulmala, M., Dada, L., Daellenbach, K.R., Yan, C., Stolzenburg, D., Kontkanen, J., Ezhova, E., Hakala, S., Tuovinen, S., Kokkonen, T.V., Kurppa, M., Cai, R., Zhou, Y., Yin, R., Baalbaki, R., Chan, T., Chu, B., Deng, C., Fu, Y., Ge, M., He, H., Heikkinen, L., Junninen, H., Liu, Y., Lu, Y., Nie, W., Rusanen, A., Vakkari, V., Wang, Y., Yang, G., Yao, L., Zheng, J., Kujansuu, J., Kangasluoma, J., Petäjä, T., Paasonen, P., Järvi, L., Worsnop, D., Ding, A., Liu, Y., Wang, L., Jiang, J., Bianchi, F., Kerminen, V., 2021. Is reducing new particle formation a plausible solution to mitigate particulate air pollution in Beijing and other Chinese megacities? Faraday Discuss 226, 334–347.

Lee, S., Gordon, H., Yu, H., Lehtipalo, K., Haley, R., Li, Y., Zhang, R.(, 2019. New particle formation in the atmosphere: from molecular clusters to global climate. J. Geophys. Res. Atmos. 124, 7098–7146. https://doi.org/10.1029/2018JD029356.

Lei, L., Zhou, W., Chen, C., He, Y., Li, Z., Sun, J., Tang, X., Fu, P., Wang, Z., Sun, Y., 2020. Long-term characterization of aerosol chemistry in cold season from 2013 to 2020 in Beijing, China. Environ. Pollut. 115952. https://doi.org/10.1016/j.envpol.2020.115952.

Li, Z., Xia, X., Cribb, M., Mi, W., Dickerson, R.E.(, 2007. Aerosol optical properties and their radiative effects in northern China. J. Geophys. Res. Atmos. 112, 321–341. https://doi.org/10.1029/2006JD007382.

Li, Z., Lau, W.K.M., Ramanathan, V., Wu, G., Ding, Y., Manoj, M.G., Liu, J., Qian, Y., Li, J., Zhou, T., Fan, J., Rosenfeld, D., Ming, Y., Wang, Y., Huang, J., Wang, B., Xu, X., Lee, S.S., Cribb, M., Zhang, F., Yang, X., Zhao, C., Takemura, T., Wang, K., Xia, X., Yin, Y., Zhang, H., Guo, J., Zhai, P.M., Sugimoto, N., Babu, S.S., Brasseur, G. P.(, 2016. Aerosol and monsoon climate interactions over Asia. Rev. Geophys. 54, 866–929. https://doi.org/10.1002/2015RG000500.

Li, Y.J., Sun, Y., Zhang, Q., Li, X., Li, M., Zhou, Z., Chan, C.K., 2017. Real-time chemical characterization of atmospheric particulate matter in China: a review, *Atmos.* Environ 158, 270–304. https://doi.org/10.1016/j.atmosenv.2017.02.027.

Li, Z., Guo, J., Ding, A., Liao, H., Liu, J., Sun, Y., Wang, T., Xue, H., Zhang, H., Zhu, B.(, 2017. Aerosol and boundary-layer interactions and impact on air quality. Natl. Sci. Rev. 4, 810–833. https://doi.org/10.1093/nsr/nwx117.

Li, H., Cheng, J., Zhang, Q., Zheng, B., Zhang, Y., Zheng, G., He, K., 2019. Rapid transition in winter aerosol composition in Beijing from 2014 to 2017: response to clean air actions. Atmos. Chem. Phys. 19 (11) https://doi.org/10.5194/acp-19-11485-2019, 485–11,499.

Li, Z., Wang, Y., Guo, J., Zhao, C., Cribb, M.C., Dong, X., Fan, J., Gong, D., Huang, J., Jiang, M., Jiang, Y., Lee, S.S., Li, H., Li, J., Liu, J., Qian, Y., Rosenfeld, D., Shan, S., Sun, Y., Wang, H., Xin, J., Yan, X., Yang, X., Yang, X., Zhang, F., Zheng, Y.(, 2019. East Asian study of tropospheric aerosols and their impact on regional clouds, precipitation, and climate (EAST-AIR$_{CPC}$). J. Geophys. Res. Atmos. 124 (13) https://doi.org/10.1029/2019JD030758, 026–13,054.

Liang, C., Wu, H., Li, H., Zhang, Q., Li, Z., He, K., 2020. Efficient data preprocessing, episode classification, and source apportionment of particle number concentrations. Sci. Total Environ. 744, 140923. https://doi.org/10.1016/j.scitotenv.2020.140923.

Matus, K., Nam, K., Selin, N.E., Lamsal, L.N., Reilly, J.M., Paltsev, S., 2012. Health damages from air pollution in China. Global Environ. Change 22, 55–66. https://doi.org/10.1016/j.gloenvcha.2011.08.006.

Peng, J.F., Hu, M., Wang, Z.B., Huang, X.F., Kumar, P., Wu, Z.J., Guo, S., Yue, D.L., Shang, D.J., Zheng, Z., He, L.Y.(, 2014. Submicron aerosols at thirteen diversified sites in China: size distribution, new particle formation and corresponding contribution to cloud condensation nuclei production. Atmos. Chem. Phys. 14 (10) https://doi.org/10.5194/acp-14-10249-2014, 249–10,265.

Peng, J., Hu, M., Shang, D., Wu, Z., Du, Z., Tan, T., Wang, Y., Zhang, F., Zhang, R., 2021. Explosive secondary aerosol formation during severe haze in the north China plain. Environ. Sci. Technol. 55, 2189–2207.

Rivas, I., Beddows, D.C.S., Amato, F., Green, D.C., Järvi, L., Hueglin, C., Reche, C., Timonen, H., Fuller, G.W., Niemi, J.V., Pérez, N., Aurela, M., Hopke, P.K., Alastuey, A., Kulmala, M., Harrison, R.M., Querol, X., Kelly, F.J.(, 2020. Source apportionment of particle number size distribution in urban background and traffic stations in four European cities. Environ. Int. 135, 105345. https://doi.org/10.1016/j.envint.2019.105345.

Roldin, P., Ehn, M., Kurten, T., Olenius, T., Rissanen, M.P., Sarnela, N., Elm, J., Rantala, P., Hao, L., Hyttinen, N., Heikkinen, L., Worsnop, D.R., Pichelstorfer, L., Xavier, C., Clusius, P., Ostrom, E., Petaja, T., Kulmala, M., Vehkamaki, H., Virtanen, A., Riipinen, I., Boy, M., 2019. The role of highly oxygenated organic molecules in the boreal aerosol-cloud-climate system. Nat. Commun. 10 https://doi.org/10.1038/s41467-019-12338-8.

Rosenfeld, D., Lohmann, U., Raga, G.B., O'Dowd, C.D., Kulmala, M., Fuzzi, S., Reissell, A., Andreae, M.O., 2008. Flood or drought: how do aerosols affect precipitation? Science 321, 1309. https://doi.org/10.1126/science.1160606.

Shi, Z., Vu, T., Kotthaus, S., Harrison, R.M., Grimmond, S., Yue, S., Zhu, T., Lee, J., Han, Y., Demuzere, M., Dunmore, R.E., Ren, L., Liu, D., Wang, Y., Wild, O., Allan, J., Acton, W.J., Barlow, J., Barratt, B., Beddows, D., Bloss, W.J., Calzolai, G., Carruthers, D., Carslaw, D.C., Chan, Q., Chatzidiakou, L., Chen, Y., Crilley, L., Coe, H., Dai, T., Doherty, R., Duan, F., Fu, P., Ge, B., Ge, M., Guan, D., Hamilton, J.F., He, K., Heal, M., Heard, D., Hewitt, C.N., Hollaway, M., Hu, M., Ji, D., Jiang, X., Jones, R., Kalberer, M., Kelly, F.J., Kramer, L., Langford, B., Lin, C., Lewis, A.C., Li, J., Li, W., Liu, H., Liu, J., Loh, M., Lu, K., Lucarelli, F., Mann, G., McFiggans, G., Miller, M.R., Mills, G., Monk, P., Nemitz, E., O'Connor, F., Ouyang, B., Palmer, P.I., Percival, C., Popoola, O., Reeves, C., Rickard, A.R., Shao, L., Shi, G., Spracklen, D., Stevenson, D., Sun, Y., Sun, Z., Tao, S., Tong, S., Wang, Q., Wang, W., Wang, X., Wang, X., Wang, Z., Wei, L., Whalley, L., Wu, X., Wu, Z., Xie, P., Yang, F., Zhang, Q., Zhang, Y., Zhang, Y., Zheng, M., 2019. Introduction to the special issue"In-depth study of air pollution sources and processes within Beijing and its surrounding region (APHH-Beijing),". Atmos. Chem. Phys. 19, 7519–7546. https://doi.org/10.5194/acp-19-7519-2019.

Shrivastava, M., Cappa, C.D., Fan, J., Goldstein, A.H., Guenther, A.B., Jimenez, J.L., Kuang, C., Laskin, A., Martin, S.T., Ng, N.L., Petaja, T., Pierce, J.R., Rasch, P.J., Roldin, P., Seinfeld, J.H., Shilling, J., Smith, J.N., Thornton, J.A., Volkamer, R., Wang, J., Worsnop, D.R., Zaveri, R.A., Zelenyuk, A., Zhang, Q., 2017. Recent advances in understanding secondary organic aerosol: implications for global climate forcing. Rev. Geophys. 55, 509–559. https://doi.org/10.1002/2016RG000540.

Stolzenburg, D., Simon, M., Ranjithkumar, A., Kürten, A., Lehtipalo, K., Gordon, H., Ehrhart, S., Finkenzeller, H., Pichelstorfer, L., Nieminen, T., He, X.C., Brilke, S., Xiao, M., Amorim, A., Baalbaki, R., Baccarini, A., Beck, L., Bräkling, S., Caudillo Murillo, L., Chen, D., Chu, B., Dada, L., Dias, A., Dommen, J., Duplissy, J., El Haddad, I., Fischer, L., Gonzalez Carracedo, L., Heinritzi, M., Kim, C., Koenig, T.K., Kong, W., Lamkaddam, H., Lee, C.P., Leiminger, M., Li, Z., Makhmutov, V., Manninen, H.E., Marie, G., Marten, R., Müller, T., Nie, W., Partoll, E., Petäjä, T., Pfeifer, J., Philippov, M., Rissanen, M.P., Rörup, B., Schobesberger, S., Schuchmann, S., Shen, J., Sipilä, M., Steiner, G., Stozhkov, Y., Tauber, C., Tham, Y. J., Tomé, A., Vazquez-Pufleau, M., Wagner, A.C., Wang, M., Wang, Y., Weber, S.K., Wimmer, D., Wlasits, P.J., Wu, Y., Ye, Q., Zauner-Wieczorek, M., Baltensperger, U., Carslaw, K.S., Curtius, J., Donahue, N.M., Flagan, R.C., Hansel, A., Kulmala, M., Lelieveld, J., Volkamer, R., Kirkby, J., Winkler, P.M., 2020. Enhanced growth rate of atmospheric particles from sulfuric acid. Atmos. Chem. Phys. 20, 7359–7372.

Su, T., Li, Z., Li, C., Li, J., Han, W., Shen, C., Tan, W., Wei, J., Guo, J., 2020. The significant impact of aerosol vertical structure on lower atmosphere stability and its critical role in aerosol-planetary boundary layer (PBL) interactions. Atmos. Chem. Phys. 20, 3713–3724. https://doi.org/10.5194/acp-20-3713-2020.

Vu, D., Gao, S., Berte, T., Kacarab, M., Yao, Q., Vafai, K., Asa-Awuku, A.(, 2019. External and internal cloud condensation nuclei (CCN) mixtures: controlled laboratory studies of varying mixing states. Atmos. Meas. Tech. 12, 4277–4289. https://doi.org/10.5194/amt-12-4277-2019.

Wang, L.T., Wei, Z., Yang, J., Zhang, Y., Zhang, F.F., Su, J., Meng, C.C., Zhang, Q., 2013. The 2013 severe haze over the southern Hebei, China: model evaluation, source apportionment, and policy implications. Atmos. Chem. Phys. Discuss. 13.

Wang, G., Zhang, R., Gomez, M.E., Yang, L., Zamora, M.L., Hu, M., Lin, Y., Peng, J., Guo, S., Meng, J., 2016. Persistent sulfate formation from London Fog to Chinese haze. Proc. Natl. Acad. Sci. U. S. A 113 (13), 630–13,635.

Wang, Y., Zhang, F., Li, Z., Tan, H., Xu, H., Ren, J., Zhao, J., Du, W., Sun, Y., 2017. Enhanced hydrophobicity and volatility of submicron aerosols under severe emission control conditions in Beijing. Atmos. Chem. Phys. 17, 5239–5251. https://doi.org/10.5194/acp-17-5239-2017.

Wang, Z., Wu, Z., Yue, D., Shang, D., Guo, S., Sun, J., Ding, A., Wang, L., Jiang, J., Guo, H., 2017. New particle formation in China: current knowledge and further directions. Sci. Total Environ. 577, 258–266.

Wang, Y., Li, Z., Zhang, Y., Du, W., Zhang, F., Tan, H., Xu, H., Fan, T., Jin, X., Fan, X., Dong, Z., Wang, Q., Sun, Y., 2018. Characterization of aerosol hygroscopicity, mixing state, and CCN activity at a suburban site in the central North China Plain. Atmos. Chem. Phys. 18 (11) https://doi.org/10.5194/acp-18-11739-2018, 739–11,752.

Wang, Y., Li, Z., Zhang, R., Jin, X., Xu, W., Fan, X., Wu, H., Zhang, F., Sun, Y., Wang, Q., Cribb, M., Hu, D.(, 2019. Distinct ultrafine- and accumulation-mode particle properties in clean and polluted urban environments. Geophys. Res. Lett. 46 (10) https://doi.org/10.1029/2019GL084047, 918–10,925.

Wang, J., Li, J., Ye, J., Zhao, J., Wu, Y., Hu, J., Liu, D., Nie, D., Shen, F., Huang, X., Huang, D.D., Ji, D., Sun, X., Xu, W., Guo, J., Song, S., Qin, Y., Liu, P., Turner, J.R., Lee, H.C., Hwang, S., Liao, H., Martin, S.T., Zhang, Q., Chen, M., Sun, Y., Ge, X., Jacob, D.J., 2020a. Fast sulfate formation from oxidation of SO2 by NO2 and HONO observed in Beijing haze. Nat. Commun. 11, 2844.

Wang, M., Kong, W., Marten, R., He, X., Chen, D., Pfeifer, J., Heitto, A., Kontkanen, J., Dada, L., Kürten, A., Yli-Juuti, T., Manninen, H.E., Amanatidis, S., Amorim, A., Baalbaki, R., Baccarini, A., Bell, D.M., Bertozzi, B., Bräkling, S., Brilke, S., Murillo, L. C., Chiu, R., Chu, B., De Menezes, L., Duplissy, J., Finkenzeller, H., Carracedo, L.G., Granzin, M., Guida, R., Hansel, A., Hofbauer, V., Krechmer, J., Lehtipalo, K., Lamkaddam, H., Lampimäki, M., Lee, C.P., Makhmutov, V., Marie, G., Mathot, S., Mauldin, R.L., Mentler, B., Müller, T., Onnela, A., Partoll, E., Petäjä, T., Philippov, M., Pospisilova, V., Ranjithkumar, A., Rissanen, M., Rörup, B., Scholz, W., Shen, J., Simon, M., Sipilä, M., Steiner, G., Stolzenburg, D., Tham, Y.J., Tomé, A., Wagner, A.C., Wang, D.S., Wang, Y., Weber, S.K., Winkler, P.M., Wlasits, P.J., Wu, Y., Xiao, M., Ye, Q., Zauner-Wieczorek, M., Zhou, X., Volkamer, R., Riipinen, I., Dommen, J., Curtius, J., Baltensperger, U., Kulmala, M., Worsnop, D.R., Kirkby, J., Seinfeld, J.H., El-Haddad, I., Flagan, R.C., Donahue, N.M., 2020b. Rapid growth of new atmospheric particles by nitric acid and ammonia condensation. Nature 581, 184–189.

Wei, J., Li, Z., Lyapustin, A., Sun, L., Peng, Y., Xue, W., Su, T., Cribb, M.C., 2021. Reconstructing 1-km-resolution high-quality PM$_{2.5}$ data records from 2000 to 2018 in China: spatiotemporal variations and policy implications. Remote Sens. Environ. 252, 112136. https://doi.org/10.1016/j.rse.2020.112136.

Williamson, C.J., Kupc, A., Axisa, D., Bilsback, K.R., Bui, T., Campuzano-Jost, P., Dollner, M., Froyd, K.D., Hodshire, A.L., Jimenez, J.L., Kodros, J.K., Luo, G., Murphy, D.M., Nault, B.A., Ray, E.A., Weinzierl, B., Wilson, J.C., Yu, F., Yu, P., Pierce, J.R., Brock, C.A.(, 2019. A large source of cloud condensation nuclei from new particle formation in the tropics. Nature 574, 399. https://doi.org/10.1038/s41586-019-1638-9.

Wu, Z., Wang, Y., Tan, T., Zhu, Y., Li, M., Shang, D., Wang, H., Lu, K., Guo, S., Zeng, L., Zhang, Y.(, 2018. Aerosol liquid water driven by anthropogenic inorganic salts: implying its key role in haze formation over the North China Plain. Environ. Sci. Technol. Lett. 5, 160–166. https://doi.org/10.1021/acs.estlett.8b00021.

Wu, H., Li, Z., Li, H., Luo, K., Wang, Y., Yan, P., Hu, F., Zhang, F., Sun, Y., Shang, D., Liang, C., Zhang, D., Wei, J., Wu, T., Jin, X., Fan, X., Cribb, M., Fischer, M.L., Kulmala, M., Petäjä, T.(, 2020. The impact of the atmospheric turbulence-development tendency on new particle formation: a common finding on three continents. Natl. Sci. Rev. https://doi.org/10.1093/nsr/nwaa157 nwaa157.

Xiao, M., Hoyle, C.R., Dada, L., Stolzenburg, D., Kürten, A., Wang, M., Lamkaddam, H., Garmash, O., Mentler, B., Molteni, U., Baccarini, A., Simon, M., He, X.C., Lehtipalo, K., Ahonen, L.R., Baalbaki, R., Bauer, P.S., Beck, L., Bell, D., Bianchi, F., Brilke, S., Chen, D., Chiu, R., Dias, A., Duplissy, J., Finkenzeller, H., Gordon, H., Hofbauer, V., Kim, C., Koenig, T.K., Lampilahti, J., Lee, C.P., Li, Z., Mai, H., Makhmutov, V., Manninen, H.E., Marten, R., Mathot, S., Mauldin, R.L., Nie, W., Onnela, A., Partoll, E., Petäjä, T., Pfeifer, J., Pospisilova, V., Quéléver, L.L.J., Rissanen, M., Schobesberger, S., Schuchmann, S., Stozhkov, Y., Tauber, C., Tham, Y. J., Tomé, A., Vazquez-Pufleau, M., Wagner, A.C., Wanger, R., Wang, Y., Weitz, L., Wimmer, D., Wu, Y., Yan, C., Ye, P., Ye, Q., Zha, Q., Zhou, X., Amorim, A., Carslaw, K., Curtius, J., Hansel, A., Volkamer, R., Winkler, P.M., Flagan, R.C., Kulmala, M., Worsnop, D.R., Kirkby, J., Donahue, N.M., Baltensperger, U., El

Haddad, I., Dommen, J., 2021. The driving factors of new particle formation and growth in the polluted boundary layer. Atmos. Chem. Phys. Discuss. 2021, 1–28.
Yao, L., Garmash, O., Bianchi, F., Zheng, J., Yan, C., Kontkanen, J., Junninen, H., Mazon, S.B., Ehn, M., Paasonen, P., Sipilä, M., Wang, M., Wang, X., Xiao, S., Chen, H., Lu, Y., Zhang, B., Wang, D., Fu, Q., Geng, F., Li, L., Wang, H., Qiao, L., Yang, X., Chen, J., Kerminen, V., Petäjä, T., Worsnop, D.R., Kulmala, M., Wang, L., 2018. Atmospheric new particle formation from sulfuric acid and amines in a Chinese megacity. Science 361, 278. https://doi.org/10.1126/science.aao4839.
Zhai, S., Jacob, D.J., Wang, X., Shen, L., Li, K., Zhang, Y., Gui, K., Zhao, T., Liao, H., 2019. Fine particulate matter (PM2.5) trends in China, 2013–2018: separating contributions from anthropogenic emissions and meteorology. Atmos. Chem. Phys. 19 (11) https://doi.org/10.5194/acp-19-11031-2019, 031–11,041.
Zhang, Y., Dore, A.J., Ma, L., Liu, X.J., Ma, W.Q., Cape, J.N., Zhang, F.S., 2010. Agricultural ammonia emissions inventory and spatial distribution in the North China Plain. Environ. Pollut. 158, 490–501.
Zhang, F., Wang, Y., Peng, J., Ren, J., Collins, D., Zhang, R., Sun, Y., Yang, X., Li, Z., 2017. Uncertainty in predicting CCN activity of aged and primary aerosols. J. Geophys. Res. Atmos. 122 (11) https://doi.org/10.1002/2017JD027058, 711–723, 736.
Zhang, Y., Du, W., Wang, Y., Wang, Q., Wang, H., Zheng, H., Zhang, F., Shi, H., Bian, Y., Han, Y., Fu, P., Canonaco, F., Prévôt, A.S.H., Zhu, T., Wang, P., Li, Z., Sun, Y., 2018. Aerosol chemistry and particle growth events at an urban downwind site in North China Plain. Atmos. Chem. Phys. 18 (14) https://doi.org/10.5194/acp-18-14637-2018, 637–14,651.
Zhang, Q., Zheng, Y., Tong, D., Shao, M., Wang, S., Zhang, Y., Xu, X., Wang, J., He, H., Liu, W., Ding, Y., Lei, Y., Li, J., Wang, Z., Zhang, X., Wang, Y., Cheng, J., Liu, Y., Shi, Q., Yan, L., Geng, G., Hong, C., Li, M., Liu, F., Zheng, B., Cao, J., Ding, A., Gao, J., Fu, Q., Huo, J., Liu, B., Liu, Z., Yang, F., He, K., Hao, J., 2019. Drivers of improved $PM_{2.5}$ air quality in China from 2013 to 2017. Proc. Natl. Acad. Sci. U. S. A. 116 (24) https://doi.org/10.1073/pnas.1907956116, 463–24,469.
Zhang, F., Wang, Y., Peng, J., Chen, L., Sun, Y., Duan, L., Ge, X., Li, Y., Zhao, J., Liu, C., Zhang, X., Zhang, G., Pan, Y., Wang, Y., Zhang, A.L., Ji, Y., Wang, G., Hu, M., Molina, M.J., Zhang, R.(, 2020. An unexpected catalyst dominates formation and radiative forcing of regional haze. Proc. Natl. Acad. Sci. U. S. A 117, 3960. https://doi.org/10.1073/pnas.1919343117.
Zheng, G.J., Duan, F.K., Su, H., Ma, Y.L., Cheng, Y., Zheng, B., Zhang, Q., Huang, T., Kimoto, T., Chang, D., Pöschl, U., Cheng, Y.F., He, K.B., 2015. Exploring the severe winter haze in Beijing: the impact of synoptic weather, regional transport and heterogeneous reactions. Atmos. Chem. Phys. 15, 2969–2983.
Zheng, B., Tong, D., Li, M., Liu, F., Hong, C., Geng, G., Li, H., Li, X., Peng, L., Qi, J., 2018. Trends in China's anthropogenic emissions since 2010 as the consequence of clean air actions. Atmos. Chem. Phys. 18 (14), 095–14,111.